IEEE Photonics Journal
An IEEE Photonics Society Publication

Open Access

Design and Comparison of SF57 Over SiO_2 on Same Structured PCF for Residual Dispersion Compensation

Volume 8, Number 6, December 2016

Russel Reza Mahmud
Muhammad Abdul Goffar Khan
S. M. Abdur Razzak

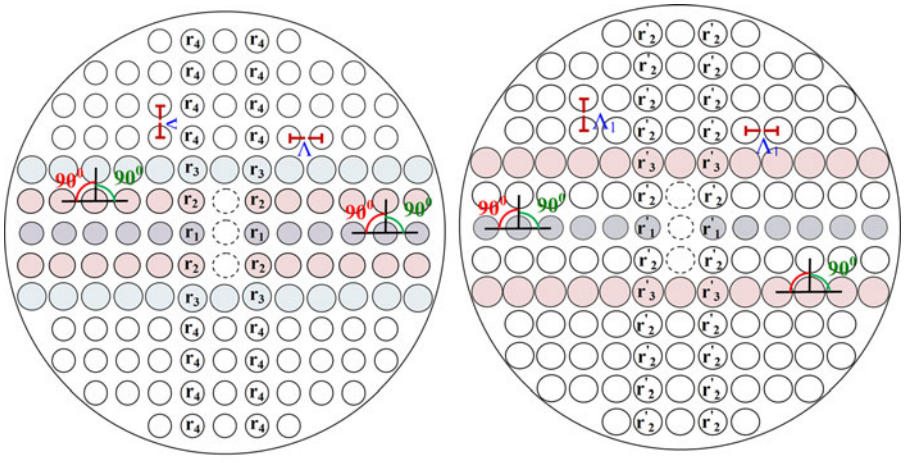

DOI: 10.1109/JPHOT.2016.2628802
1943-0655 © 2016 IEEE

IEEE photonics SOCIETY

IEEE

Design and Comparison of SF57 Over SiO_2 on Same Structured PCF for Residual Dispersion Compensation

Russel Reza Mahmud, Muhammad Abdul Goffar Khan, and S. M. Abdur Razzak

Department of Electrical and Electronic Engineering, Rajshahi University of Engineering & Technology, Rajshahi 6204, Bangladesh.

DOI:10.1109/JPHOT.2016.2628802

Manuscript received July 26, 2016; revised October 24, 2016; accepted November 8, 2016. Date of publication November 17, 2016; date of current version December 12, 2016. Corresponding author: Russel Reza Mahmud (e-mail: r.r.mahmud@gmail.com).

Abstract: Two square photonic crystal fibers (SPCFs), one made of silica (SiO_2) and the other made of high index lead silicate soft glass (SF57), are numerically analyzed, compared, and proposed in this paper. Both designs of SPCFs show very high negative and ultraflattened chromatic dispersion with very low variation of dispersion (ΔD). P-1 offers $-650(\pm 6)$ ps/(nm.km) for the wavelength range of $1.46 \rightarrow 1.63\ \mu$m and bandwidth (BW) $= 170$ nm and P-2 offers $-693(\pm 4)$ ps/(nm.km) for the wavelength range of $1.45 \rightarrow 1.68\ \mu$m (BW $= 230$ nm) with average high birefringence of the order of 10^{-2}. The proposed designs can be suitable for residual dispersion compensation while maintaining polarization due to having the properties of high negative flattened chromatic dispersion with high birefringence. The influence of changing the structural parameters up to $\pm 0.02\mu$m are also examined for ensuring the flatness of the property of chromatic dispersion within the acceptable level.

Index Terms: Square photonic crystal fiber, polarization maintaining residual dispersion compensation, negative flattened chromatic dispersion, high birefringence.

1. Introduction

Photonic crystal fibers (PCFs) possess several expedient characteristics for which they have depicted immense recognition in the field of optical fiber. A PCF for residual dispersion compensation (R-DC) with maintaining polarization is one of the most crucial aspects for application [2], [4]–[6] in optical data transmission system (O-DTS). Generally, a standard single mode optical fiber (SSMOF) used in conventional O-DTS exhibits positive chromatic dispersion (C-D) of 12 to 22 ps/(nm.km) [2], [4]. This C-D reaches to a huge positive margin with a high peak large magnitude when an optical signal travels a very long distance in a fiber [2]. Since this positive dispersion deteriorates the performance of the optical pulse signal, it should be diminished. A dispersion compensation fiber (with very high sloping negative dispersion) needs to link with the conventional SSMOF to minimize the huge positive dispersion. Unfortunately, after every dispersion compensation, the residual dispersion always remains in a BW. Therefore, the system requires additional compensation to nullify the extra residual dispersion that can be done by linking a residual dispersion compensation (R-DC) fiber. This R-DC fiber provides flattened negative chromatic dispersion (FNC-D). A PCF should be tailored as much as the high negative and ultra-flattened chromatic dis-

persion property to reduce costs and all losses [6]. In O-DTS, for polarization maintaining purposes, the property of high birefringence (*B*) in PCF is required. Therefore, a PCF with the dual characteristics (FNC-D and *B*) will be a perfect applicant as a fiber for the use of polarization maintaining residual dispersion compensation [4], [6].

Considering these theories, several researchers demonstrated PCFs on high FNC-D for addressing the issue of R-DC over the course of time [3]. For instance, some artificially created elliptical cores in hybrid octagonal structures were reported in [2] and [4], which showed FNC-D of $-465.5(\pm 5.25)$ and $-562(\pm 6)$ ps/(nm.km) for the wavelength (hereinafter represented as WL) range of, respectively, $1.46 \rightarrow 1.675$ μm and $1.46 \rightarrow 1.7$ μm. Nevertheless, these two reported designs [2], [4] are same in structure and are not purely octagonal. However, all the construction of the PCFs make the models impractical to set up the air holes near the core region with specified shapes and dimension for formation. Again, a hybrid decagonal [3] PCF that confirms FNC-D of $-558.96(\pm 4.85)$ ps/(nm.km) for the WL range of $1.46 \rightarrow 1.7$ μm. This design is also complex to form using conventional stack and draw method (CSDM) for being hybrid decagonal structure. A conventional common pattern called hexagonal in the [5] exhibited FNC-D of $-456(\pm 6)$ ps/(nm.km) within WL range of $1.37 \rightarrow 1.7$ μm. The prime disadvantage of [5] is a very small hexagonal PCF is designed into another hexagonal PCF in a solo structure which is impractical to form employing CSDM. An uncommon pentagonal structure (almost impossible to form through CSDM) in ref. no. 6 ensured FNC-D of $-611.9(\pm 6.1)$ ps/(nm.km) between the WL range of $1.46 \rightarrow 1.625$ μm. Futhermore, equiangular decagonal spiral PCFs in [6] and [7] discovered FNC-D of $-337.5(\pm 7.5)$ ps/(nm.km) and $-453(\pm 7)$ ps/(nm.km) within the WL range of, respectively, $1.35 \rightarrow 1.65$ μm and $1.15 \rightarrow 1.75$ μm. Owing to the pattern of spiral, the designs in [7] and [8] are complicated to form through the CSDM. Besides, the structure of 7 is more difficult for placing an elliptical air hole in the core region that makes the design as a slotted pattern. A conventional octagonal structure [9] made of SiO_2 reported FNC-D of -708 ps/(nm.km) with dispersion variation ($\triangle$D) of 20 ps/(nm.km) for the WL range of $1.46 \rightarrow 1.67$ μm. The design has high negative dispersion. Neverthless, for having $\triangle D = 20$ ps/(nm.km), it is not flattened well to work as an R-DC fiber properly. Very recently a square PCF offers high negative slop dispersion of -2500 ps/(nm.km) at 1.55 μm WL which can be used for dispersion compensation purposes [17]. In 2004, a square PCF offered chromatic dispersion of 50 to -200 ps/(nm.km) for the WL range of $1.2 \rightarrow 1.6$ μm [18]. Moreover, dispersion of 35 to -180 ps/(nm.km) for $1.2 \rightarrow 2.0$ μm WL was proposed by another square PCF in 2009 [13]. So far as we know, there is no PCF on square structure reported the property of FNC-D for the application of residual dispersion compensation.

Hence, ultra-flattened very high negative dispersion of two new square (S) structure PCF designs with high birefringence are proposed and compared in this monograph. The SiO_2 made SPCF (hereinafter represented as P-1) offers FNC-D of -644 to -656 ps/(nm.km) with $\triangle$D of 12 ps/(nm.km) for $1.46 \rightarrow 1.63$ μm (BW $= 170$ nm), whereas high index lead silicate soft glass (SF57) made SPCF (also represented as P-2) performs -689 to -697 ps/(nm.km) with $\triangle$D of 8 ps/(nm.km) for $1.45 \rightarrow 1.68$ μm (BW $= 230$ nm) with average high *B* of the order 10^{-2} for that offered bandwidth. The BW of P-1 involves S, C, L, and P-2 involves the S, C, L, and U bands for the optical third window into the infrared region. In O-DTS, residual dispersion compensation with maintaining polarization is the applicable field for any of the P-1 and P-2 SPCFs having their properties.

2. Structure and Design of the Proposed SPCF

We propose a simple square structure PCFs have investigated by two different materials. one is SiO_2 and other is SF57. SiO_2 is very common, available and popular material for designing PCF. On the other hand, SF57 has higher refractive index (*n*) than SiO_2 and that confines the light into the central core location for wider WL range. Besides, SF57 is also available and exhibits good thermal and crystallization stability [8]. The cross sectional view of the SiO_2 based P-1 SPCF and SF57 based P-2 SPCF with optimum design parameters (ODP), straight line numbers, and dimensions are displayed in Fig. 1(a) and (b), respectively. The designs are in square pattern in the central core region. The SPCF has seven straight lines in the upper and lower portion of the y-axis. The

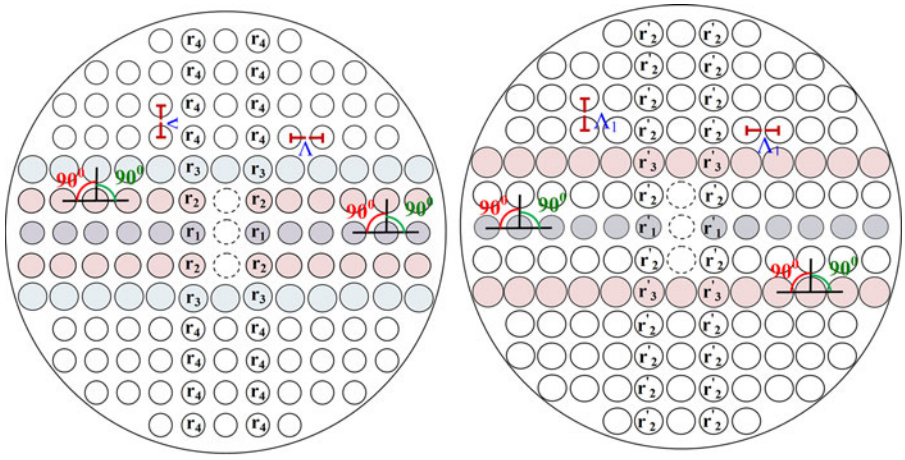

Fig. 1. Cross sectional view of the P-1 SPCF (a) and P-2 SPCF (b) with symbols and different colors of the diameters of air holes for each straight line, angle between air holes, pitch, and omitted air holes in details.

air holes' diameters have the same value in the longitudinal x-axis. The only dependent variable of the proposed design is pitch that is denoted as Λ for P-1 and Λ_1 for P-2. This pitch is a distance between any two consecutive air holes on any axis within the same or different square pattern and it controls all the variables. The angle between two air holes is 90° and that is why any four air holes can generate a square. We intentionally omit three air holes in the core location from the first and second straight lines along the up and down position of the y-axis for obtaining high birefringence which are reported circular dotted lines in Fig. 1. Four types (r_1, r_2, r_3, and r_4) and three types (r'_1, r'_2, and r'_3) of circular air holes are used, respectively, for P-1 and P-2. In P-1, the air holes' diameters in the first, second, third, and fourth to seventh straight lines along the upper and lower portion of the y-axis are denoted respectively as r_1, r_2, r_3 and r_4. For P-2, r'_1, r'_3 and r'_2 depict the circular air holes' diameters, respectively, in the first, third, and the rest of the straight lines along the upper and lower portions of the vertical y-axis. For optimization, both the structures of P-1 and P-2 have equal value of pitch that is equal to $\Lambda = \Lambda_1 = 0.49\ \mu$m. The ODP of the air holes in P-1 are $r_1 = 0.72 \times \Lambda$, $r_2 = 0.78 \times \Lambda$, $r_3 = 0.87 \times \Lambda$ and $r_4 = 0.75 \times \Lambda$. Likewise, in P-2, the ODP are $r'_1 = 0.72 \times \Lambda_1$, $r'_2 = 0.85 \times \Lambda_1$ and $r'_3 = 0.95 \times \Lambda_1$. In addition, the P-1 and P-2 have, respectively, five and four variables, including pitch and diameters of air holes into the whole structure. Therefore, in comparison between these two structures regarding parameters, P-2 is more simple than P-1 for having less variables. In optimization procedure, we observe the influence for changing one parameter when others are fixed, which are analyzed and reported in the figures.

3. Equations, Results of Simulation and Discussion

The guiding properties of both the proposed SPCFs have been observed by popular COMSOL software which is dependent on finite element method. A perfectly matched absorbing boundary layer in circular pattern which has no reflection, is used to find the confinement loss or leakage loss (L_C). Triangular vector edge elements of 4152 and 4480 and a mesh area of about 72.27 and 72.27 μm^2, respectively, are used to calculate the modal properties of the P-1 and P-2 SPCFs. The fundamental equation for the full vector finite element method can be expressed as (1), show below, where E, K_0, and Λ represent electric field vector, wave number, and WL. The FEM directly solves Maxwell's equation to find out the most approximate value of the effective refractive index (n_{eff}). Afterwards, waveguide dispersion (D_w) can be evaluated by (2), shown below, having the unit of ps/(nm.km). In that equation, C represent in vacuum the light velocity. The refractive index (n)

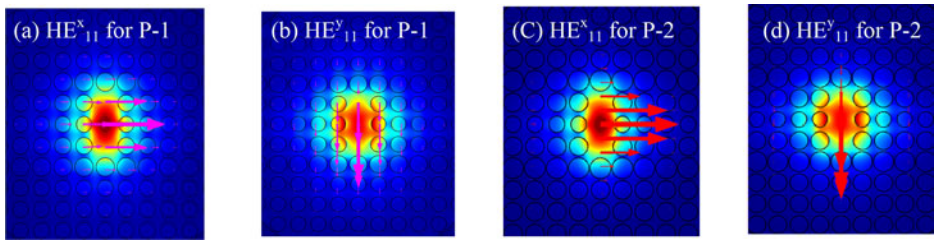

Fig. 2. Field pattern in optical form of the fundamental x-polarization mode (HE$^{x}_{11}$) and y-polarization mode (HE$^{y}_{11}$) at the WL of 1.55 μm for the P-1 and P-2 SPCF designs. (a), (c) HE$^{x}_{11}$ mode (b), (d) HE$^{y}_{11}$ mode.

of the SiO_2 can be obtained by the Sellmeier equation (3), shown below, where the value of Sellmeier constants are $B_1 = 0.6961663$, $B_2 = 0.4079426$, $B_3 = 0.8974794$, $C_1 = 0.004679148$, $C_2 = 0.01351206307$ and $C_3 = 97.93400254$. Likewise, to define n of SF57, the sellmeier constant are $B_1 = 1.81651371$, $B_2 = 0.428893641$, $B_3 = 1.07186278$, $C_1 = 0.0143704198$, $C_2 = 0.0592801172$, and $C_3 = 121.419942$. After getting n of SiO_2 and SF57, the material dispersion (D_m) can be calculated by (4), shown below. Total chromatic dispersion (D_t) can be evaluated by (5), shown below. Birefringence is an important property which is defined as B, where, n^{x}_{eff} and n^{y}_{eff} are real part of the mode indices of the two fundamental x-y polarization modes represent as respectively HE$^{x}_{11}$ and HE$^{y}_{11}$. L_C can be obtained in dB/m by (7), shown below, where imaginary part of n_{eff} needs to put into equation. Besides, the effective area (A_{eff}) has the unit of μm^2 is calculated by (8), shown below, where electric field is need to put into Maxwell's equation. Nonlinear coefficient (γ) is obtained from (9), shown below, where the Kerr constant (n_2) for SiO_2 is 2.1×10^{-20} m^2W^{-1} [9] and for SF57 is 4.1×10^{-19} m^2W^{-1} [1]. The unit of γ is $W^{-1}km^{-1}$. The effective V parameter (V_{eff}) is calculated by the (10), shown below, where Λ is the pitch, n_{eff} represents effective refractive index, and n_a represents refractive index of the air holes. The free space wave number $K_0 = (2\pi/\lambda)$. In that equation, air filling fraction is represented as $F = A_{hole}/A_{cell}$. Here, A_{hole} and A_{cell} are the area of holes and PCF, respectively, [10].

$$\nabla \times (\mu_r^{-1} \nabla \times E) - k_0[\varepsilon_r]E = 0 \tag{1}$$

$$D_w = -(\lambda/C)\left[\left(d^2 \,\mathrm{Re}[n_{eff}]\right)/d\lambda^2\right] \tag{2}$$

$$n = \sqrt{1 + \frac{B_1\lambda^2}{\lambda^2 - C_1} + \frac{B_2\lambda^2}{\lambda^2 - C_2} + \frac{B_3\lambda^2}{\lambda^2 - C_3}} \tag{3}$$

$$D_m = -(\lambda/C)\left[\left(d^2 n\right)/d\lambda^2\right] \tag{4}$$

$$D_t = D_w + D_m \tag{5}$$

$$B = \left|\mathrm{Re}(n^{X}_{eff}) - \mathrm{Re}(n^{Y}_{eff})\right| \tag{6}$$

$$L_C = 8.686 \times k_O \,\mathrm{Im}[n_{eff}] \tag{7}$$

$$A_{eff}(\lambda) = \left[\int_{-\infty}^{\infty}\int_{-\infty}^{\infty}\left(|E(x,y)|^2\right)dxdy\right]^2 \Big/ \int_{-\infty}^{\infty}\int_{-\infty}^{\infty}\left(|E(x,y)|^4 dxdy\right) \tag{8}$$

$$\gamma = (2\pi/\lambda)(n_2/A_{eff}) \tag{9}$$

$$V_{eff} = (k_0 \Lambda F^{1/2})({n_{eff}}^2 - {n_a}^2)^{1/2}. \tag{10}$$

The optical field distributions for the WL at 1.55 μm of the fundamental x- polarized mode (HE$^{x}_{11}$) and y-polarization mode (HE$^{y}_{11}$) are given in the Fig. 2. It can be noticed from the simulation in Fig. 2 that at the central core region the light is strongly confined since the cladding part has lower refractive index than the core. Since SF57 has higher n than SiO_2, the strong mode confinement

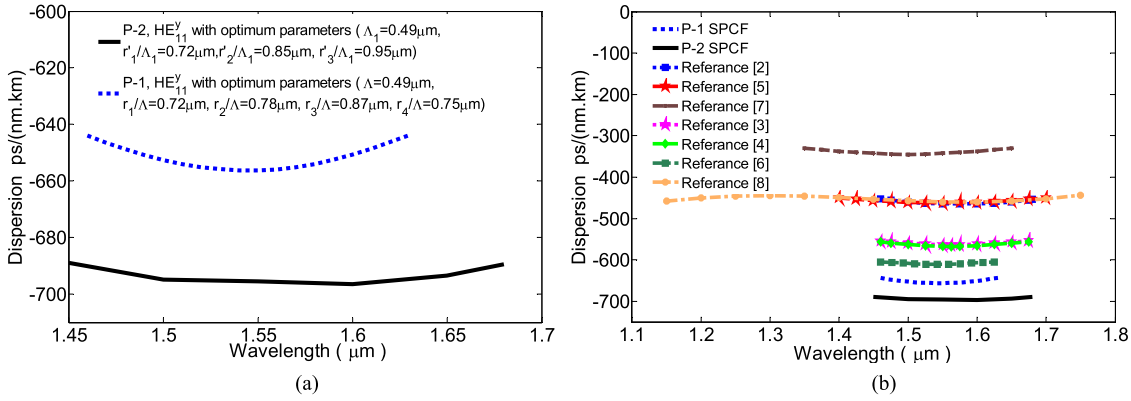

Fig. 3. D_t with respect to WL. (a) P-1 covers S + C + L and P-2 covers S + C + L + U bands with ODP. (b) shows flatness at negative level of P-1 and P-2 SPCF with some recent results of the reported designs in references.

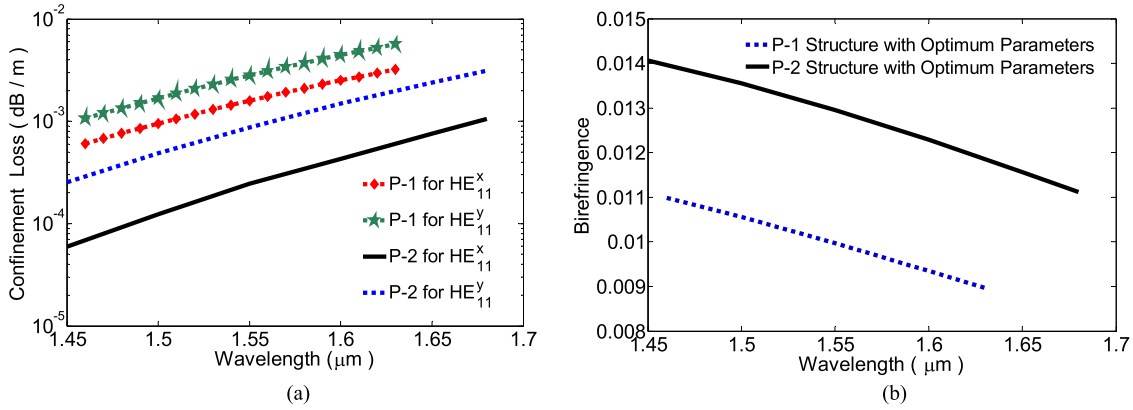

Fig. 4. (a) L_C with respect to WL for HE$^x_{11}$ and HE$^y_{11}$ modes with ODP for P-1 (with emblems) and P-2 (without emblems). (b) B with respect to WL with ODP (without emblems solid line for P-2 and dashed line for P-1 SPCF).

is more easily possible in the core of P-2 than P-1. Artificially created asymmetrical core pattern offers higher n^x_{eff} for HE$^x_{11}$ than n^y_{eff} for HE$^y_{11}$. HE$^y_{11}$ mode sits in a large core area (see Fig. 2(b) and (d)), and hence, it is well confined while the power of HE$^x_{11}$ mode leaks into the adjacent air holes (see Fig. 2(a) and (c)). That is why L_C of HE$^y_{11}$ is higher than HE$^x_{11}$, which is shown in Fig. 4(a). From the simulation, it has been found that total power have passed into the solid material and cladding air holes for HE$^x_{11}$ is about 73.4% and 26.6% and for HE$^y_{11}$ is about 68% and 32%. Since power fraction into cladding air holes for HE$^x_{11}$ is comparatively lower than HE$^y_{11}$, therefore, HE$^x_{11}$ exhibits higher n_{eff} than HE$^y_{11}$. It is also observed from the results of simulation that the n_{eff} of the HE$^x_{11}$ and HE$^y_{11}$ are decreased with increasing of the WL.

A true R-DC fiber should have high FNC-D as well as very shot in length for minimizing costs and losses. Fig. 3(a) shows very high and ultra FNC-D for both P-1 and P-2 are, respectively, −644 to −656 and −689 to −697 ps/(nm.km) with absolute ΔD of 12 and 8 ps/(nm.km) within the WL range of 1.46 → 1.63 μm and 1.45 → 1.68 μm for HE$^y_{11}$. At best, from our literature review, chromatic dispersion is considered to be well flattened if ΔD is within the limit of 12 ps/(nm.km) [2]–[5], [8]. Fig. 3(b) views comparison at a glance between our proposed P-1 and P-2 and different structures reported by researchers [2]–[8] regarding D_t with the function of the WL. Therefore, we do not consider the designs of the [9] for a comparison at a glance in Fig. 3(b) which has ΔD

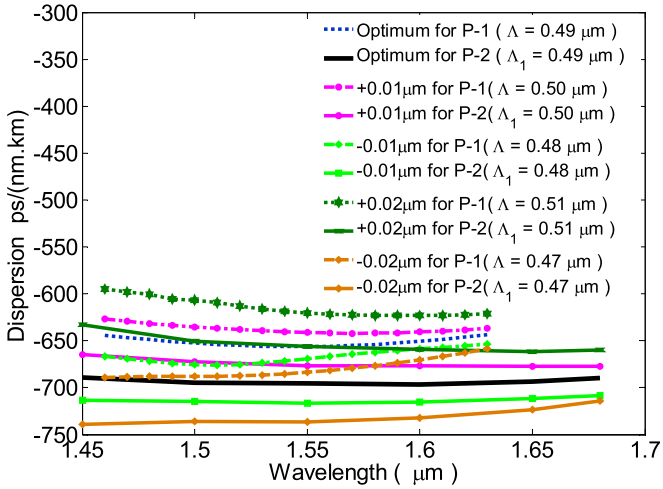

Fig. 5. D_t effects with respect to WL for alteration of only pitch (Λ for P-1 and Λ_1 for P-2) when other parameters are stayed fixed. (Without emblem ODP is depicted by solid and dashed lines for, respectively, P-2 and P-1. In addition, with emblem increment and decrement of pitch for P-2 and P-1 are indicated by solid and dashed lines).

equal to or greater than 20 ps/(nm.km) within a band [9] since is not perfect enough for RDC. The proposed P-1 and P-2 provide dispersion variation of 12 and 8 ps/(nm.km), respectively, involving S + C + L and S + C + L + U bands. It is evident from Fig. 3(b) that both of our P-1 and P-2 designs confirm ultra-flattened chromatic dispersion with highest amplitude of all reported designs in references 2 to 8. Besides, the P-2 SPCF shows ultra-flattened characteristics of D_t than the references 3 to 8. A good R-DC fiber should have low L_C for a WL boundary. Fig. 4(a) confirms that L_C with respect to the WL for HE^x_{11} and HE^y_{11} of both P-1 and P-2 is very low compared to the [2] to [8]. For P-1, L_C provides the value of 10^{-3} to $10^{-2.5}$ and $10^{-3.25}$ to $10^{-2.75}$ dB/m, respectively, for the HE^y_{11} and HE^x_{11}. In the case of P-2, a much lower L_C of $10^{-3.6}$ to $10^{-2.75}$ and $10^{-4.3}$ to $10^{-3.4}$ dB/m respectively for HE^y_{11} and HE^x_{11}. It is seen from Fig. 4(b) that B of 0.015 to 0.01 and 0.0142 to 0.0115 of HE^y_{11} can be obtained for the WL range of, respectively, 1.46 $\rightarrow$ 1.63 μm and 1.45 $\rightarrow$ 1.68 μm for P-1 and P-2 with ODP. This high birefringence can maintain polarization.

For proposing a new PCF design, we need to evaluate the sensitivity of the PCF properties (mainly chromatic dispersion ensuring its flatness) for the alteration of $\pm$(0.01 to 0.02) μm in air holes' diameters and pitch which may vary during formation process from the ODP [2]–[9]. The responses of pitch variation are shown in Fig. 5, where D_t changes slightly. Dispersion varies $\pm$20 to $\pm$10 ps/(nm.km) at the edge of lower to higher WL for both P-1 and P-2 because of changing pitch by $\pm$0.01 μm when other parameters are kept unchanged. Again, we found alteration of D_t of $\pm$50 to $\pm$20 ps/(nm.km) at the edge of 1.46 $\rightarrow$ 1.63 μm for P-1 and $\pm$45 to $\pm$25 ps/(nm.km) at the edge of 1.45 $\rightarrow$ 1.68 μm for P-2 for the variation of pitch at $\pm$0.02 μm. Dispersion varies more at the edge of 1.46 μm than 1.63 μm for P-1 and 1.45 than 1.68 μm for P-2. Fig. 6 explores that for both P-1 and P-2, D_t varies by only $\pm$10 to $\pm$20 ps/(nm.km) for variation of r_1 and r'_1 of $\pm$(0.01 to 0.02) μm in the first straight line within their specified WL range. Fig. 7 shows that in the case of P-1, D_t changes $\pm$30 to $\pm$60 ps/(nm.km) for alteration of r_2 only by $\pm$(0.01 to 0.02) μm within the BW, but variation of r_2 degrades the flatness of D_t. On the other side, in the case of P-2, D_t changes only $\pm$5 to $\pm$10 ps/(nm.km) for changing of r'_2 by $\pm$(0.01 to 0.02) μm. For both P-1 and P-2, due to the variation of r_3 and r'_3, variation of D_t changes very little amount and that is shown in the Fig. 8. In case of P-1 only, the alteration of r_4 when all others ODP are kept fixed. D_t varies $\pm$30 to $\pm$60 ps/(nm.km) from the ODP within the specified BW of WL. Finally, it is remarkable that for the variation of both air holes' diameters and pitch, both the P-1 and P-2 maintain the characteristics of the FNC-D and that satisfies the formation tolerance. Compared to P-1, P-2 performs the dispersion flatness more

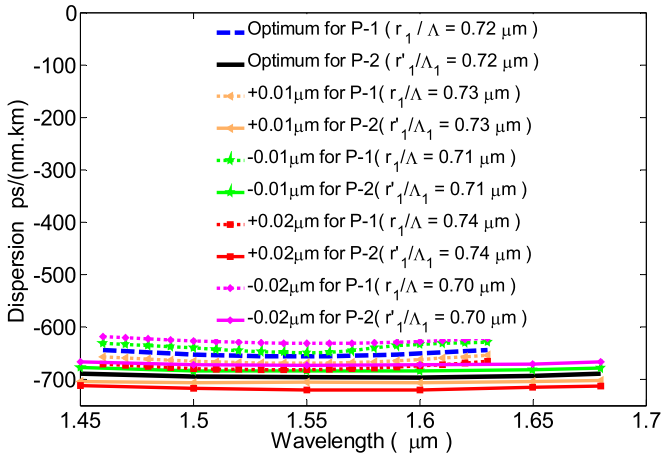

Fig. 6. D_t effects with respect to WL for alteration of only r_1 for P-1 and r'_1 for P-2. (Without emblem ODP is explored by solid and dashed line for P-2 and P-1. Furthermore, with emblem increment and decrement of r'_1 and r_1 for P-2 and P-1 are displayed by other solid and dashed lines).

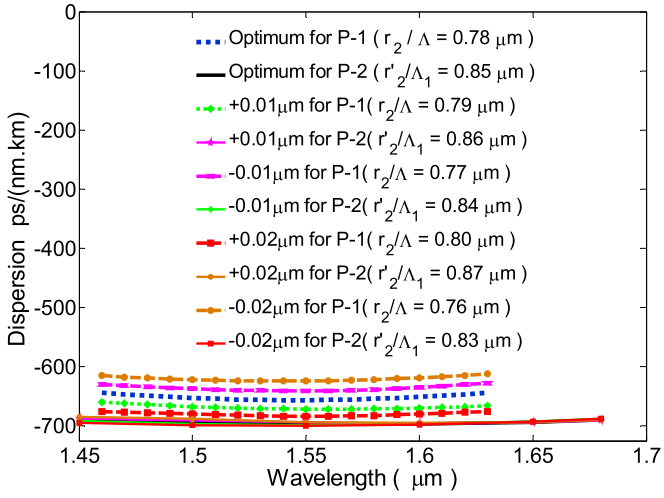

Fig. 7. D_t effects with respect to WL for alteration of only r_2 for P-1 and r'_2 for P-2. (Without emblem ODP for P-2 and P-1 is explored by solid and dashed lines, and with emblem increment and decrement of r'_2 and r_2 for P-2 and P-1 are shown by solid and dashed lines).

accurately and confirms higher amplitude of negative flattened dispersion with small dispersion variation. Therefore, P-2 performs better than P-1 considering D_t.

From the data of the results of simulation, the effective area (A_{eff}) is found 1.11 to 1.36 μm^2 for P-1 and 0.95 to 1.22 μm^2 for P-2, respectively, within the WL range of 1.46 $\rightarrow$ 1.63 μm and 1.45 $\rightarrow$ 1.68 μm with ODP. When the WL is increased, the A_{eff} is also increased. Since, the A_{eff} of the fiber is very small and the HE^x_{11} and HE^y_{11} are tightly confined, the nonlinear phenomenon such as stimulated brillouin scattering and four wave mixing may be raised noises into the fiber material when high intensity of light propagates. This may limit such fiber for using high power pulse delivery application. The RD-C fiber generally used in O-DTS to compensate the residual dispersion, where high FNC-D leads small length of a fiber to compensate the residual dispersion. The proposed fiber provides very high FNC-D and high B which can work perfectly in O-DTS using a short fiber length [16]. Besides, this high FNC-D can suppress the nonlinear parametric process of a fiber [4]. The splice loss (L_s) is generally high since for being smaller A_{eff} for the proposed

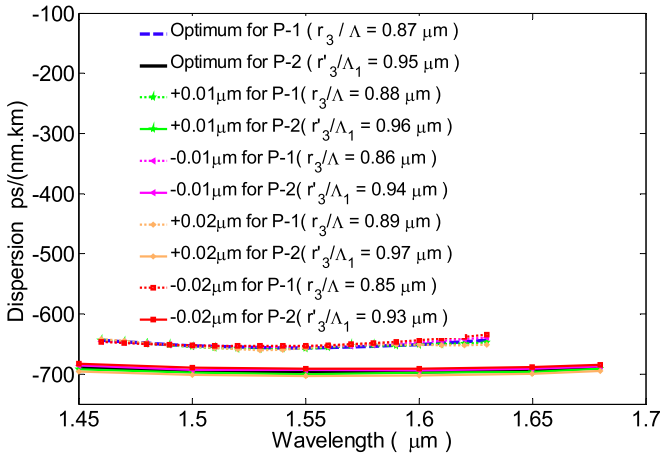

Fig. 8. D_t effects with respect to WL for alteration of only r_3 for P-1 and r'_3 for P-2 when other parameters are kept constant. (Here, without emblem ODP for P-2 and P-1 are reported by solid and dashed lines. Nevertheless, with emblem decrement and increment of r'_3 and r_3 are indicated by solid lines for P-2 and dashed lines for P-1).

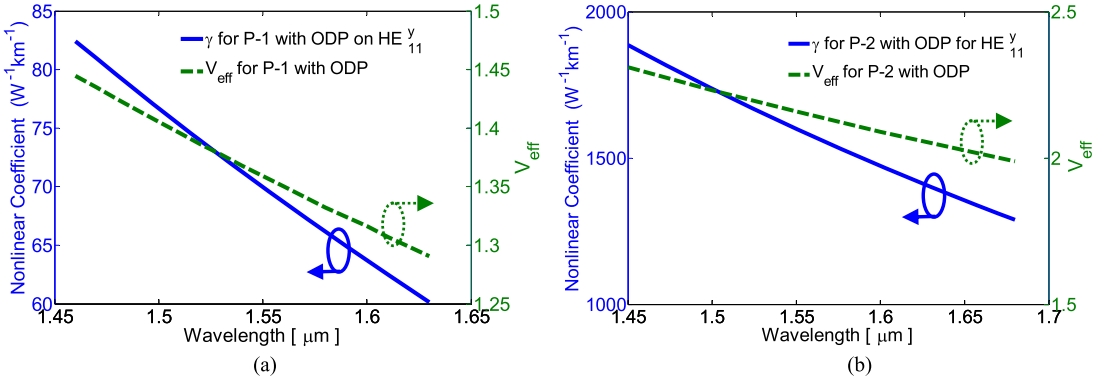

Fig. 9. γ and V_{eff} parameter with respect to the WL for P-1 (a) and P-2 (b) of the SPCF designs.

P-1 and P-2. Recently, special techniques have been proposed by many researchers to minimize L_s in the coupling between conventional SSMOF and PCF. Fusion splicing [12] (invented by Xiao *et al.*) is a technique that can reduce L_s. A new splice-free coupling technique is proposed by L. Saval *et al.* [11] which can reduce L_s for coupling purpose between conventional SSMOF and any structure of PCF.

For the analysis of mode test, the investigation is studied carefully that both the proposed P-1 and P-2 report a stronger fundamental mode (HE_{11}^y) than the second mode (3968 and 9707 times stronger for P-1 and P-2, respectively) at 1.55 μm WL. In addition, the L_C of the second mode is higher than (HE_{11}^y) and that is more than 46 dB/m [2], [4], [8], [10]. Therefore, both the proposed P-1 and P-2 SPCF will successfully operate as a single-mode fiber [5]–[7], [9]. Moreover, for the single mode analysis by applying another method, the effective V parameter (V_{eff}) is calculated by equation (10) [10]. Fig. 9 reports that both the P-1 and P-2 can be performed as a single mode fiber for the WL range of 1.46 $\rightarrow$ 1.63 μm and 1.45 $\rightarrow$ 1.68 μm since V_{eff} is less than the numerical value of 1.5 and 2.4 or π within that bandwidth. Fig. 9 also exhibits γ of 70 and 1599.8 $W^{-1}km^{-1}$ for P-1 and P-2 at 1.55 μm WL. The property of high γ is necessary for supercontinuum generation, optical parametric amplification, and in nonlinear optics application. Now considering the formation issue, both the proposed P-1 and P-2 square SPCF designs with circular air holes can

TABLE 1
Comparison the Properties at 1.55 μm WL Between the Proposed (P-1 and P-2) With Other PCF Designs

Ref.	WL Range (μm)	FNC-D	ΔD	B	γ	Arrangement of Air Holes
[2]	1.46 $\rightarrow$ 1.675	-458.5	13	10^{-2}	–	Elliptical core in hybrid octagonal structure
[3]	1.46 $\rightarrow$ 1.7	-558.5	9.7	10^{-2}	–	Elliptical-circular hybrid decagonal
[4]	1.46 $\rightarrow$ 1.7	-562	12	10^{-2}	50	Elliptical core in hybrid octagonal structure
[5]	1.37 $\rightarrow$ 1.7	-456	12	10^{-7}	12	PCF in PCF in hexagonal
[6]	1.46 $\rightarrow$ 1.625	-611.6	12.2	10^{-2}	45	Pentagonal
[7]	1.35 $\rightarrow$ 1.65	-337.5	15	10^{-3}	–	Elliptical-circular slotted hybrid decagonal spiral
[8]	1.15 $\rightarrow$ 1.75	-453	14	10^{-2}	–	Decagonal spiral
P-1	**1.46 $\rightarrow$ 1.63**	**-650**	**12**	$\mathbf{10^{-2}}$	**70**	**SiO_2 made square**
P-2	**1.45 $\rightarrow$ 1.68**	**-693**	**8**	$\mathbf{10^{-2}}$	**1599.8**	**SF57 made square**

be formed by using the stack and draw procedure, which is explained in detail in [13]. In addition, a new ultrasonic drilling machine can be used to form any complex holey structure [14]. Besides, the sol-gel technique can be applied [15], providing flexibility to form any PCF of various irregular structures. Using this method [15], any complex structure has been already formed. Table 1 shows the comparison between the proposed (P-1 and P-2) and other PCFs' design with data, results, and analysis.

4. Conclusion

Two SPCFs (P-1 and P-2) have been proposed, and they offer very high negative flattened dispersion of -650 ($\Delta D = 12$) ps/(nm.km) within the wavelength range of 1.46 $\rightarrow$ 1.63 μm (BW = 170 nm) for P-1 and -693 ($\Delta D = 8$) ps/(nm.km) within 1.45 $\rightarrow$ 1.68 μm (BW = 230 nm) wavelength range for P-2 with high birefringence of the order 10^{-2}. In addition, it demonstrates very low confinement loss of the order of 10^{-3} to $10^{-2.5}$ dB/m for P-1 and $10^{-3.6}$ to $10^{-2.75}$ dB/m for P-2 within the bandwidth of interest. Among these two proposed designs with the same structure, P-2 (SF57 made SPCF) confirms better results than P-1 (SiO_2 made SPCF) in all respects. Owing to the excellent properties, both the proposed (P-1 and P-2) SPCFs will be promising applicants for residual dispersion compensation with polarization maintaining application in optical systems.

References

[1] A. Agrawal, N. Kejalakshmy, B. M. A. Rahman, and K. T. V. Grattan, "Soft glass equiangular spiral photonic crystal fiber for super continuum generation," *IEEE Photon. Technol. Lett.*, vol. 21, no. 22, pp. 1722–1724, Nov. 2009.
[2] M. Samiul Habib, R. Ahmad, M. Selim Habib, and M. I. Hasan, "Residual dispersion compensation over S + C + L + U wavelength bands using highly birefringent octagonal photonic crystal fiber," *Appl. Opt.*, vol. 53, no. 14, pp. 3057–3062, May 2014.
[3] M. S. Habib and E. Khandker, "Highly birefringent photonic crystal fiber with ultra-flattened negative dispersion over S + C + L + U bands," *Appl. Opt.*, vol. 54, no. 10, pp. 2786–2789, 2015.
[4] M. I. Hasan, S. M. A. Razzak, and M. S. Habib, "Design and characterization of highly birefringent residual dispersion compensating photonic crystal fiber," *J. Lightw. Technol.*, vol. 32, no. 23, pp. 3976–3982, Dec. 2014.
[5] D. C. Tee, M. H. A. Bakar, N. Tamchek, and F. R. M. Adikan, "Photonic crystal fiber in photonic crystal fiber for residual dispersion compensation over E + S + C + L + U wavelength bands," *IEEE Photon. J.*, vol. 5, no. 3, Jun. 2013, Art. no. 7200607.
[6] X. Li, P. Liu, Z. Xu, and Z. Zhang, "Design of a pentagonal photonic crystal fiber with high birefringence and large flattened negative dispersion," *Appl. Opt.*, vol. 54, no. 24, pp. 7350–7357, Aug. 2015.

[7] M. A. Islam and M. S. Alam., "Design optimization of equiangular spiral photonic crystal fiber for large negative flat dispersion and high birefringence," *J. Lightw. Technol.*, vol. 30, no. 22, pp. 3545–3551, Nov. 2012.
[8] R. R. Mahmud, S. M. A. Razzak, M. I. Hasan, and G. K. M. Hasanuzzaman, "Ultraflattened high negative chromatic dispersion over O + E + S + C + L + U bands of a microstructured optical fiber," *Opt. Eng.*, vol. 54, no. 9, pp. 0971051–0971057, Sep. 2015.
[9] R. R. Mahmud, M. A. G. Khan, and S. M. A. Razzak, "Management of residual dispersion of an optical transmission system using octagonal photonic crystal fiber," *Opt. Eng.*, vol. 55, no. 4, pp. 0471071–0471077, Apr. 2016.
[10] S. M. A. Razzak and Y. Namihira, "Proposal for highly nonlinear dispersion-flattened octagonal photonic crystal fibers," *IEEE Photon. Technol. Lett.*, vol. 20, no. 4, pp. 249–251, Feb. 2008.
[11] S. G. L. Saval *et al.*, "Splice-free interfacing of photonic crystal fibers," *Opt. Lett.*, vol. 30, no. 13, pp. 629–1631, Jul. 2005.
[12] L. Xiao, W. Jin, and M. S. Demokan, "Fusion splicing small core photonic crystal fibers and single-mode fibers by repeated arc discharges," *Opt. Lett.*, vol. 32, no. 2, pp. 115–117, Jan. 2007.
[13] S. Kim, C. S. Kee, and C. G. Lee, "Modified rectangular lattice photonic crystal fibers with high birefringence and negative dispersion," *Opt. Exp.*, vol. 17, no. 10, pp. 795–7957, May 2009.
[14] X. Feng, A. K. Mairaj, D. W. Hewak, and T. M. Monro, "Nonsilica glasses for holey fibers," *J. Lightw. Technol.*, vol. 23, no. 6, pp. 2046–2054, Jun. 2005.
[15] R. T. Bise and D. J. Trevor, "Sol-gel derived microstructured fibers: Fabrication and characterization," in *Proc. Int. Conf. Opt. Fiber Commun.*, Washington, DC, USA, Mar. 2005, Art. no. OWL6.
[16] L. Zhang, T. Luo, Y. Yue, and A. E. Willner, "High group birefringence in photonic crystal fibers with both positive and negative phase birefringence," *J. Opt. A Pure Appl. Opt.*, vol. 10, no. 3, Feb. 2008, Art. no. 035004.
[17] P. S. Maji and P. R. Chaudhuri, "Designing broad band dispersion compensation with square lattice PCF and applications to ASE suppression with ultra negative dispersion," *Optik*, vol. 127, no. 5, pp. 2603–2607, Mar. 2016.
[18] A. H. Bouk, A. Cucinotta, F. Poli, and S. Selleri, "Dispersion properties of square-lattice photonic crystal fibers," *Opt. Exp.*, vol. 12, no. 5, pp. 941–946, 2004.